

Deformations in $N = 14$ isotones

Y. Kanada-En'yo

Institute of Particle and Nuclear Studies, High Energy Accelerator Research Organization, Ibaraki 305-0801, Japan

(Received 23 September 2004; published 11 January 2005)

Systematic analysis of deformations in neutron-rich $N = 14$ isotones was done based on the method of antisymmetrized molecular dynamics. The property of the shape coexistence in ^{28}Si , which is known to have the oblate ground state and the prolate excited states, was successfully described. The results suggest that the shape coexistence may occur also in neutron-rich $N = 14$ nuclei as well as ^{28}Si . It was found that the oblate neutron shapes are favored because of the spin-orbit force in most of $N = 14$ isotones. Q moments and $E2$ transition strengths in the neutron-rich nuclei were discussed in relation to the intrinsic deformations, and a possible difference between the proton and neutron deformations in ^{24}Ne was proposed.

DOI: 10.1103/PhysRevC.71.014303

PACS number(s): 21.60.-n, 02.70.Ns, 21.10.Ky, 27.20.+n

I. INTRODUCTION

The shape coexistence in ^{28}Si has been studied for a long time. At the early stage, the oblate and prolate solutions of Hartree-Fock calculations are associated with the ground 0^+ state and the 0_3^+ state at 6.691 MeV, respectively [1]. Experimentally, the ground band is known to be oblate from the sign of the quadrupole moment of the 2_1^+ state [2,3], whereas the band-head 0_3^+ in the prolate band has been identified by γ transition measurements [4]. In addition to static quadrupole deformation, the nonaxial deformation and vibration of ^{28}Si have been recently studied in the detailed analysis of the inelastic scattering by use of the coupled-channel method with the soft rotator model [5].

The coexistence of oblate and prolate states in ^{28}Si can be described by the shell gap at $N = 14$ and $Z = 14$ of Nilsson orbits in the deformed system [6]. A variety of shapes is considered to arise from the nature of the shell structure in $N = 14$ and/or $Z = 14$ systems, where a half of the sd shell is occupied. It is natural to expect that shape coexistence phenomena may appear also in neutron-rich nuclei with $N = 14$. From the coexistence of oblate and prolate states in ^{28}Si , one may expect that this trend of the oblate and prolate neutron structure might survive in other $N = 14$ isotones. The primary interest in the present article is on the deformations of the proton and neutron densities in neutron excess $N = 14$ nuclei. How does the oblate neutron structure in the ground band of ^{28}Si change with the decrease of proton number toward the neutron-rich region—and whether or not the coexistence of oblate and prolate deformations occurs? The neutron deformations should be sensitive to the proton structure, therefore, the shape coexistence of the neutron structure may depend on the proton number. If an oblate neutron shape is favored also in neutron-rich nucleus as well as in ^{28}Si , one may meet another question: is the proton shape consistent with the neutron one? In this sense, ^{24}Ne is an attractive nucleus, where the proton shape would be different from the neutron shape, because the prolate shape of proton density is favored in $Z = 10$ systems as seen in ^{20}Ne .

In the study of proton and neutron deformations, the experimental data of electric moments such as $B(E2)$ are useful to extract information about the intrinsic deformations.

Recently, $B(E2; 2^+ \rightarrow 0^+)$ in ^{24}Si has been measured by Coulomb excitation [7]. The measured $B(E2)$ in ^{24}Si is almost as large as the experimental value of $B(E2)$ in ^{24}Ne . The ratio $B(E2; ^{24}\text{Si})/B(E2; ^{24}\text{Ne}) \leq 1$ is much smaller than a naive expectation based on a collective model picture that $B(E2)$ is proportional to $(N/Z)^2 \approx 2$. If these nuclei are mirror symmetric, the ratio $B(E2; ^{24}\text{Si})/B(E2; ^{24}\text{Ne}) \leq 1$ lead to a possible difference between proton and neutron deformations in ^{24}Ne .

The coexistence of the oblate and prolate solutions in ^{28}Si has been confirmed by many theoretical calculations such as Nilsson-Strutinsky calculations [8], Hartree-Fock-Bogoliubov [9], and α -cluster model approaches [10,11]. Although mean field approaches are useful for systematic study of deformations, their applicability to very light nuclei is not obvious. In the light nuclear region, we remind readers of the importance of cluster aspect, which closely relates with the deformations. The cluster aspect has been suggested also in light neutron-rich nuclei as well as stable nuclei. For example, it is well known that ^{20}Ne has an $^{16}\text{O}+\alpha$ cluster structure, whereas the development of clustering was suggested in neutron-rich B isotopes. The cluster aspect and the shape coexistence of even-even $N = Z$ nuclei has been studied by α -cluster models [10,11]. 7α -cluster model calculations were applied to ^{28}Si and successfully describe an exotic shape with D_{5h} symmetry [10,12], which is associated with the $K^\pi = 5^-$ band observed in γ transitions [4]. Although the properties of the oblate and prolate states were described by the 7α -cluster models [10,11], however, many 7α -cluster calculations failed to reproduce the order of the oblate and prolate solutions in ^{28}Si . Namely, in most of the α -cluster calculations, the prolate solutions are lower than the oblate solutions except for few calculations with Brink-Boeker forces [10]. For the oblate property of the ground state in ^{28}Si , it is important to incorporate the effect of spin-orbit force, which is omitted within the α -cluster models. Furthermore, the cluster models are not suitable for the systematic study of unstable nuclei, because they rely on the assumption of existence of cluster cores.

For the systematic structure study of light nuclei, one of the powerful approaches is the method of antisymmetrized molecular dynamics (AMD). The applicability of this method

for unstable nuclei has been proved in many works [13–16]. In addition to description of deformations and cluster aspect in light nuclei, this method has an advantage that electric moments can be directly related with structure change based on the microscopic treatment of spin-parity projection without introducing effective charges.

In this article, we study the deformations of $N = 14$ isotones while focusing on the coexistence of the oblate and prolate neutron structure. We pay attention to reproduction of the order of oblate and prolate solutions, which coexist in ^{28}Si , and discuss the effect of the spin-orbit force. We analyze the systematics of deformations in the neutron excess nuclei in relation to the observables such as Q moments and $E2$ transition strength. This article is organized as follows. In the next section, the formulation of AMD is briefly explained. We show the theoretical results and give comparisons with the experimental data in Sec. IV. In Sec. V, we analyze the intrinsic structure and discuss the lowering mechanism of the oblate state within the AMD framework. Finally, a summary is given in Sec. VI.

II. FORMULATION

Here we briefly explain the formulations of the present calculations. Details of the formulation of AMD methods for nuclear structure studies are explained in Refs. [13,15]. The present calculations are basically same as those in Ref. [13].

The wave function of a system with a mass number A is written by a superposition of AMD wave functions Φ_{AMD} . An AMD wave function is given by a single Slater determinant of Gaussian wave packets as follows:

$$\Phi_{\text{AMD}}(\mathbf{Z}) = \frac{1}{\sqrt{A!}} \mathcal{A}\{\varphi_1, \varphi_2, \dots, \varphi_A\}, \quad (1)$$

where the i th single-particle wave function is written as follows:

$$\varphi_i = \phi_{\mathbf{x}_i} \chi_i \tau_i, \quad (2)$$

$$\phi_{\mathbf{x}_i}(\mathbf{r}_j) \propto \exp \left\{ -v \left(\mathbf{r}_j - \frac{\mathbf{X}_i}{\sqrt{v}} \right)^2 \right\}, \quad (3)$$

$$\chi_i = \left(\frac{1}{2} + \xi_i \right) \chi_{\uparrow} + \left(\frac{1}{2} - \xi_i \right) \chi_{\downarrow}. \quad (4)$$

The isospin function τ_i is fixed to be up(proton) or down(neutron), and the orientation of intrinsic spin ξ_i is fixed to be $1/2$ or $-1/2$ in the present calculations as done in Ref. [13]. The spatial part is represented by complex variational parameters, X_{1i} , X_{2i} , X_{3i} , which indicate the centers of Gaussian wave packets.

In the AMD model, all the centers of single-nucleon Gaussians are treated independently as the complex variational parameters. Thus, this method is based completely on single nucleons and therefore it does not rely on the assumption of the existence of cluster cores. In the sense that a single AMD wave function is written by a Slater determinant of Gaussians, the AMD method is regarded as an extended model of Bloch-Brink cluster model [17]. Here we note that the

Gaussian center is expressed by the complex parameter \mathbf{X}_i , which contains a real part and an imaginary part. It means an extension of the model space, because the degrees of freedom are twice of the case that Gaussian centers are given by real values as in usual cluster models. If we ignore the effect of antisymmetrization, the position \mathbf{D}_i and the momentum \mathbf{K}_i of the i th single-nucleon wave packets are expressed by the real and imaginary parts of \mathbf{X}_i , respectively, as follows:

$$\begin{aligned} \mathbf{D}_i &\equiv \frac{\langle \phi_{\mathbf{x}_i} | \mathbf{r} | \phi_{\mathbf{x}_i} \rangle}{\langle \phi_{\mathbf{x}_i} | \phi_{\mathbf{x}_i} \rangle} = \frac{\text{Re}(\mathbf{X}_i)}{\sqrt{v}} \\ \mathbf{K}_i &\equiv \frac{\langle \phi_{\mathbf{x}_i} | \mathbf{p} | \phi_{\mathbf{x}_i} \rangle}{\langle \phi_{\mathbf{x}_i} | \phi_{\mathbf{x}_i} \rangle} = 2\hbar\sqrt{v} \text{Im}(\mathbf{X}_i). \end{aligned} \quad (5)$$

In the nuclear structure study with the AMD, the imaginary parts of \mathbf{Z} are essential to describe the rotation motion of the system. They are important to incorporate the effect of spin-orbit force and to describe high-spin states.

We perform energy variation for a parity-eigen state, $P^{\pm} \Phi_{\text{AMD}} \equiv \Phi_{\text{AMD}}^{\pm}$, projected from an AMD wave function by using the frictional cooling method [13]. We consider the AMD wave function obtained by the energy variation as the intrinsic state, and total-angular-momentum projection (P_{MK}^J) is performed after the variation to calculate the expectation values of operators such as energies and moments. In the present calculations, the parity projection is done before the variation, but the total-angular-momentum projection is performed after the variation. In many of $N = 14$ isotones, two local minimum solutions are found in the energy variation. In such cases, we diagonalize the Hamiltonian and norm matrices, $\langle P_{MK'}^J \Phi_{\text{AMD}}^{\pm} | H | P_{MK''}^J \Phi_{\text{AMD}}^{\pm} \rangle$ and $\langle P_{MK'}^J \Phi_{\text{AMD}}^{\pm} | P_{MK''}^J \Phi_{\text{AMD}}^{\pm} \rangle$, with respect to the obtained intrinsic wave functions ($\Phi'_{\text{AMD}}, \Phi''_{\text{AMD}}$) and the K quantum (K', K''). After the diagonalization the ground and excited bands are obtained.

The present scheme is the variation after projection with respect to the parity projection, but it is the method of the total-angular-momentum projection after the variation (PAV). If the intrinsic spin orientations of all single-particle wave functions are treated as variational parameters, the PAV calculations tend to give small intrinsic deformations. In fact, within such a framework (free intrinsic spins in a PAV framework), the AMD calculations of $N = 14$ isotones give almost spherical neutron deformations with the $d_{5/2}$ -shell closed configuration and fail to describe the excited states such as 2_1^+ and 4_1^+ in ^{28}Si . These spherical solutions are consistent with the recent results of fermionic molecular dynamics [18,19] where the wave functions are similar to those of AMD. Conversely, in a framework of the variation after spin-parity projection, intrinsic deformations are generally more pronounced as is mentioned also in Ref. [19]. The full variation after spin-parity projection with free intrinsic spins is one of the powerful tools, as shown in the study of ^{12}C [20]; however, it takes much computational time and is difficult to apply to heavier nuclei. Instead, in the present article, we perform the AMD calculations within a PAV framework in a sense of total-angular-momentum with fixed intrinsic spins.

III. INTERACTIONS

The effective nuclear interactions adopted in the present work consist of the central force, the spin-orbit force, and Coulomb force. We adopt the MV1 force [21] as the central force. The MV1 force contains a zero-range three-body force in addition to the two-body interaction. The Bartlett and Heisenberg terms are chosen to be $b = h = 0$. We use a parameter set, case 1 of MV1 force with the Majorana parameter $m = 0.62$. Concerning the spin-orbit force, the same form of the two-range Gaussian as the G3RS force [22] is adopted. The strengths of the spin-orbit force, $u_I = -u_{II} \equiv u_{Is} = 900$, and $u_{Is} = 2800$ MeV are used.

IV. RESULTS

We calculate the natural parity states of $N = 14$ nuclei, ^{19}B , ^{20}C , ^{22}O , ^{24}Ne , and ^{28}Si , with the AMD method. The width parameters $\nu = 0.145, 0.15, 0.150, 0.155$, and 0.15 are chosen for ^{19}B , ^{20}C , ^{22}O , ^{24}Ne , and ^{28}Si , respectively, for both the calculations with $u_{Is} = 900$ and $u_{Is} = 2800$ MeV so as to minimize the energy of each nucleus.

In these $N = 14$ nuclei, we find two local minimum solutions with oblate and prolate deformations of neutron density, except for the results of ^{20}C and ^{22}O with $u_{Is} = 2800$ MeV. It signifies the trend of the shape coexistence of neutron structure in the $N = 14$ isotones. The feature of the shape coexistence originates in the nature of $N = 14$ neutron structure.

After performing the total-angular-momentum projection and the diagonalization for the obtained oblate and prolate states, we obtain rotational bands, $K^\pi = 3/2_1^-$ and $3/2_2^-$ bands in ^{19}B and $K^\pi = 0_1^+$ and 0_2^+ bands in ^{24}Ne and ^{28}Si , from the two local minimum solutions. In the calculations of ^{20}C and ^{22}O with the stronger spin-orbit force $u_{Is} = 2800$ MeV, the shape coexistence phenomena disappear and only one intrinsic state is obtained by the energy variation in each nucleus. In the calculations with $u_{Is} = 2800$ MeV, the lowest states of ^{22}O and ^{24}Ne have small prolate deformations of neutron density. As mentioned later, these states with “small prolate deformations” should be classified as the “oblate” states in the analysis of the shape coexistence in $N = 14$ systems, because their properties are similar to those of the oblate states of other $N = 14$ nuclei. Therefore, in this article we call these lowest states of ^{22}O and ^{24}Ne “oblate.”

The energies of the band-head states are shown in Fig. 1. In the results with $u_{Is} = 900$ MeV, we find that oblate and prolate bands coexist in those $N = 14$ nuclei. The oblate and prolate bands are almost degenerate in ^{20}C and ^{22}O , whereas in ^{19}B , ^{24}Ne , and ^{28}Si the prolate bands are lower than the oblate ones. With the stronger spin-orbit force $u_{Is} = 2800$ MeV, the “oblate” solutions are the lowest in all of these nuclei. Namely, the ground bands have the “oblate” neutron shapes. The prolate bands appear as excited bands in ^{19}B , ^{24}Ne , and ^{28}Si . We find no prolate solutions in ^{20}C and ^{22}O in the calculation with $u_{Is} = 2800$ MeV.

The ground state of ^{28}Si is experimentally known to be oblate. The order of the oblate and prolate bands is

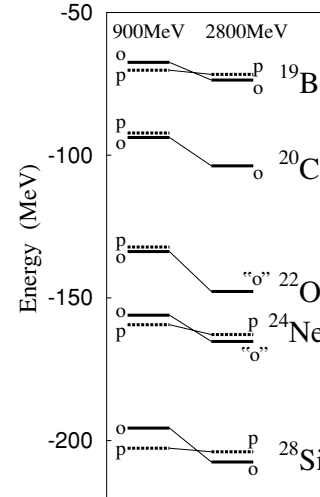


FIG. 1. Calculated binding energies for the oblate (o) and prolate (p) states. The energies are of the band-head states, $J^\pm = 3/2^-$ in ^{19}B and the 0^+ states in ^{20}C , ^{22}O , ^{24}Ne , and ^{28}Si . The results with $u_{Is} = 900$ MeV and ($u_{Is} = 2800$ MeV) are shown on the left and right, respectively. Although the “oblate” (“o”) states in ^{22}O and ^{24}Ne have small prolate deformations of neutron density, these states are attributed to the oblate neutron structure in $N = 14$ systems. The details are described in the text.

well reproduced by the calculations with $u_{Is} = 2800$ MeV. Conversely, the calculations with $u_{Is} = 900$ MeV tend to relatively overestimate the energy of the oblate bands, and they fail to reproduce the order of the oblate and prolate solutions in ^{28}Si . Comparing the results with $u_{Is} = 900$ MeV and $u_{Is} = 2800$ MeV, it is found that the relative energy of the oblate and prolate states in $N = 14$ system is very sensitive to the strength of the spin-orbit force. To describe the oblate feature of the ground state of ^{28}Si , the effect of the spin-orbit force is significant as follows. In comparison of the results for the stronger spin-orbit force ($u_{Is} = 2800$ MeV) with those for weaker one ($u_{Is} = 900$ MeV) in Fig. 1, we find that the energy gains in the oblate states are as large as about 10 MeV, whereas the energies of prolate states are almost unchanged with the increase of the strength of the spin-orbit force. As shown in Table I, the absolute value of the spin-orbit term is much larger in the oblate states than in the prolate states. It indicates that the energy gain of the spin-orbit force in the oblate state is essential to describe the level structure of ^{28}Si . The stronger spin-orbit force $u_{Is} = 2800$ is appropriate in the present framework for describing the order of the oblate and prolate levels in ^{28}Si . We discuss the lowering mechanism of the oblate states in Sec. V. Next, we show the level scheme obtained with $u_{Is} = 2800$ MeV in Fig. 2.

In ^{19}B , we predict the coexistence of oblate and prolate bands. In the previous AMD calculations of B isotopes [13], the prolate shape in the ground state was predicted in ^{19}B . This is because the adopted spin-orbit force was too weak in the previous calculations. Conversely, when we use the stronger spin-orbit force, which reproduces the order of the oblate and prolate bands in ^{28}Si , we obtain the ground state of ^{19}B with the oblate neutron shape, whereas the prolatly deformed state

TABLE I. Expectation values (MeV) of the spin-orbit force in the oblate and prolate states obtained with $u_{ls} = 2800$ MeV. Each value is for the band-head state obtained by spin-parity projection from a single AMD wave function which corresponds to "oblate" or prolate solution. The superposition of the oblate and prolate solutions is not done.

| | ^{19}B | ^{20}C | ^{22}O | ^{24}Ne | ^{28}Si |
|-----------|-----------------|-----------------|-----------------|------------------|------------------|
| "oblate" | -15.9 | -18.8 | -22.2 | -17.9 | -23.9 |
| "prolate" | -2.6 | — | — | -9.9 | -2.0 |

appears above the ground state. As shown later, the excited prolate band has $^{11}\text{Li}+^8\text{He}$ -like cluster structure. Although the 2-neutron separation energy of ^{19}B is very small at about 0.1 MeV, we expect that the prolate states may exist as resonances because such cluster states might be stable against neutron decays.

In ^{22}O , we obtain the ground state but find no other excited states in the present calculations. This is because of the double

shell-closed feature of ^{22}O . Namely, the intrinsic state has mostly spherical shape among the $N = 14$ nuclei due to the effects of the neutron $d_{5/2}$ -subshell closure and the proton magic number $Z = 8$.

In the results of ^{24}Ne , the lowest "oblate" band in the theoretical results corresponds to the ground band of experimental data as discussed in the next section. Conversely, the excited prolate bands are not experimentally identified yet. In the present calculations, a side band $K^\pm = 2^+$ of the oblate ground is suggested in addition to the excited prolate band.

In ^{28}Si , the shape coexistence of the oblate ground band and the prolate excited band has been known. The prolate band, which starts from the band-head 0_3^+ state at 6.691 MeV, has been identified in γ -transition measurements [4]. The 0_2^+ state at 4.979 MeV in the experimental data is considered to be a vibrational excitation in the oblate state. In Fig. 2, we display the experimental levels of ^{28}Si only for the positive-parity rotational bands that were assigned by $E2$ transitions [4]. The level structure of the oblate and prolate bands are reproduced by the present calculations. The level spacing between oblate and prolate bands can be reproduced in good agreement by using a slightly stronger spin-orbit force $u_{ls} = 3200$ MeV, which gives 7.3 MeV excitation energy for the band-head state of the prolate band.

The binding energies calculated with $u_{ls} = 2800$ MeV and the experimental data are shown in Fig. 3. The results with the present parameter set ($m = 0.62$, $u_{ls} = 2800$ MeV) tend to underestimate the experimental binding energies. We can fit the experimental data by choosing a smaller Majorana parameter m as usually done. For example, the result of ^{28}Si

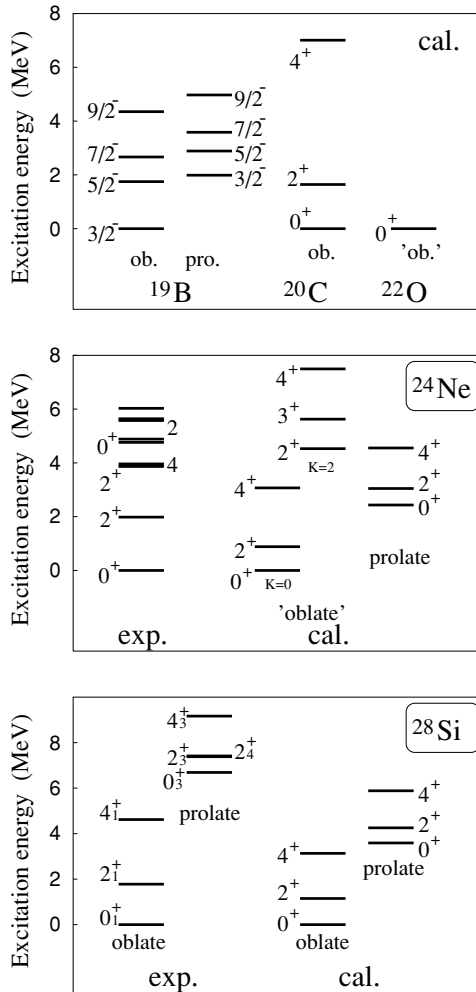


FIG. 2. The level structure of ^{19}B , ^{20}C , ^{22}O , ^{24}Ne , and ^{28}Si calculated with $u_{ls} = 2800$ MeV. The experimental data of ^{28}Si are only those in the positive-parity rotational bands that were assigned by $E2$ transitions [4].

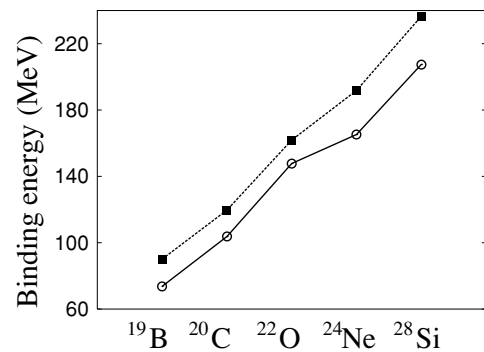


FIG. 3. Binding energies of ^{19}B , ^{20}C , ^{22}O , ^{24}Ne , and ^{28}Si . Open circles indicate the theoretical results calculated with $u_{ls} = 2800$ MeV. The experimental data are shown by square points.

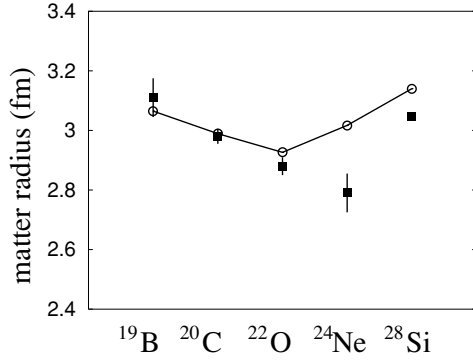


FIG. 4. Root-mean-square matter radii. Open circles indicate the radii of the lowest states calculated with $u_{ls} = 2800$ MeV. The experimental data are shown by square points. The data for ^{19}B , ^{20}C , ^{22}O , and ^{24}Ne are those derived from the interaction cross sections [23], and the radius of ^{28}Si is derived from the charge radius taken from Ref. [24] measured by electron scattering.

with $m = 0.60$ reproduces the experimental binding energy. We found that this parameter change gives only minor effects on other observables and also on the shape coexistence phenomena.

The theoretical results of the root-mean-square matter radii, $E2$ transition strengths, and electric and magnetic moments are shown in Fig. 4 and Tables II and III in comparison with the experimental data. The present calculations agree reasonably with the experimental data.

V. DISCUSSION

In this section, we analyze the deformations of proton and neutron densities in the intrinsic states and discuss their effects on the observables such as $E2$ transitions. The following discussions are based on the calculations with $u_{ls} = 2800$ MeV.

TABLE III. Electric quadrupole moments and magnetic dipole moments. The theoretical results are calculated with $u_{ls} = 2800$ MeV.

| | | Cal. | Exp. |
|------------------|--|------|----------|
| ^{28}Si | $Q(2_1^+) (e^2 \text{fm}^4)$ | 132 | 160(3) |
| | $\mu(2_1^+) (\mu_N)$ | 1.03 | 1.12(18) |
| ^{19}B | $Q(3/2_1^-; \text{oblate}) (e^2 \text{fm}^4)$ | 34 | |
| | $Q(3/2_2^-; \text{prolate}) (e^2 \text{fm}^4)$ | 43 | |
| | $\mu(3/2_1^-; \text{oblate}) (\mu_N)$ | 2.37 | |
| | $\mu(3/2_2^-; \text{prolate}) (\mu_N)$ | 2.46 | |

A. Intrinsic deformations

As mentioned before, two local minimum states are obtained in each system except for ^{20}C and ^{22}O . The deformation parameters β , γ for neutron and proton densities in the intrinsic states are shown in Fig. 5. The definition of β , γ are given in Ref. [26]. Figure 6 shows the distribution of matter, proton, and neutron densities. As shown in Figs. 5 and 6, the lowest states of ^{19}B , ^{20}C , and ^{28}Si have oblate neutron shapes. Although the lowest states of ^{22}O and ^{24}Ne have small prolate deformations of neutron densities, we notice that the characteristics of the neutron structure in these states are rather similar to those in the oblate states of other $N = 14$ nuclei. One of the remarkable features of the ‘‘oblate’’ neutron structure is the larger energy gain of the spin-orbit force than the prolate neutron structure. In fact, the energy gains of the spin-orbit force in these states of ^{22}O and ^{24}Ne are as large as those in the oblate states in ^{19}B , ^{20}C , and ^{28}Si as seen in Fig. 1 and Table I. It is considered that the oblately deformed neutron structure is not rigid but is somehow soft to vary into the small prolate deformation in such systems as ^{22}O and ^{24}Ne , which have the spherical and prolate proton shapes, respectively. In other words, the oblate neutron deformations can be modified because of the inconsistency with the proton deformations. It should be stressed that the

TABLE II. $E2$ transition strengths. The results are calculated with $u_{ls} = 2800$ MeV. The theoretical $B(E2)$ in ^{24}Si are evaluated by assuming mirror symmetry with ^{24}Ne . The experimental data are taken from Refs. [4,7,25].

| | | Cal. | | | Exp. |
|------------------|-------------|------------------------------|-----------------|------------------------------------|-----------------------|
| Band | Transitions | $B(E2)$ (w.u.) | Band | $E_i \rightarrow E_f$ | $B(E2)$ (w.u.) |
| ^{28}Si | oblate | $B(E2; 2^+ \rightarrow 0^+)$ | $K^\pi = 0_1^+$ | $1.779 \rightarrow 0$ | 12.9 ± 0.5 |
| | | $B(E2; 4^+ \rightarrow 2^+)$ | $K^\pi = 0_1^+$ | $4.617 \rightarrow 1.779$ | $13.6(+1.4, -1.2)$ |
| | prolate | $B(E2; 2^+ \rightarrow 0^+)$ | $K^\pi = 0_2^+$ | $9.164 \rightarrow (7.381, 7.417)$ | $43.5(+11.6, -8.7)^a$ |
| | | $B(E2; 4^+ \rightarrow 2^+)$ | | | |
| ^{24}Ne | ‘‘oblate’’ | $B(E2; 2^+ \rightarrow 0^+)$ | $K^\pi = 0_1^+$ | $1.981 \rightarrow 0$ | 6.8 ± 2.9 |
| | prolate | $B(E2; 2^+ \rightarrow 0^+)$ | | | |
| ^{24}Si | ‘‘oblate’’ | $B(E2; 2^+ \rightarrow 0^+)$ | $K^\pi = 0_1^+$ | $1.88 \rightarrow 0$ | 4.6 ± 1.4 |
| | prolate | $B(E2; 2^+ \rightarrow 0^+)$ | | | |
| ^{20}C | oblate | $B(E2; 2^+ \rightarrow 0^+)$ | | | |

^aBecause the collective $4^+ \rightarrow 2^+$ transition in the $K^\pi = 0_2^+$ band of ^{28}Si is distributed over two transitions into $2^+(7.381)$ and $2^+(7.417)$, the experimental value in this table is a sum of the strengths of those two transitions in Ref. [4].

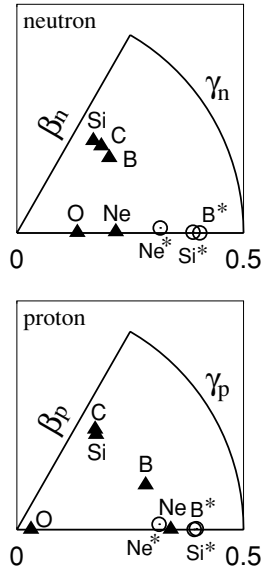


FIG. 5. Deformation parameters of the intrinsic states $\Phi_{\text{AMD}}(\mathbf{Z})$ obtained with $u_{ls} = 2800$ MeV. The deformation parameters $\beta_n, \gamma_n(\beta_p, \gamma_p)$ for the neutron (proton) densities are plotted in both panels. Triangles denote the deformations in the ground bands of ^{19}B , ^{20}C , ^{22}O , ^{24}Ne , and ^{28}Si , whereas circles indicate those in the excited bands of $^{19}\text{B}^*$, $^{24}\text{Ne}^*$, and $^{28}\text{Si}^*$.

features of the shape coexistence of neutron structure in $N = 14$ nuclei vary depending on the proton number.

In ^{19}B , the lowest state has the oblate neutron shape and a triaxial proton shape, whereas in the excited state the large prolate deformation with a cluster structure is enhanced. As seen in Fig. 6, the developed $^8\text{He}+^{11}\text{Li}$ -like clustering is suggested in the prolate excited band.

In the lowest state of ^{20}C , both the proton and neutron shapes are oblate. The reason for the absence of the prolate solution in ^{20}C is understood as follows. As known in ^{12}C , the proton shape is oblate in $Z = 6$ nuclei. Because of the inconsistency with the oblate proton deformation, the prolate neutron structure is energetically unfavored comparing with the oblate neutron structure.

In ^{22}O , the neutron deformation is the smallest among these $N = 14$ isotones due to the spherical proton shape that originates in the p -shell closure effect. Another local minimum solution with the large prolate deformation of neutron structure does not appear as well as in ^{20}C .

In ^{24}Ne , two local minimum solutions with different neutron structures are obtained. The neutron structure of the lowest state has a smaller prolate deformation than that of the excited state. This smaller neutron deformation in the lowest state can be attributed to the oblate neutron structure in $N = 14$ systems, because as mentioned above the sensitivity of the energy of this state to the strength of the spin-orbit force is quite similar to that of the oblate states in other $N = 14$ isotones. Conversely, in the excited state, the neutron structure has a large prolate deformation and is similar to the prolate excited state of ^{28}Si . Therefore, the coexistence of two local minimum solutions in ^{24}Ne is associated with the shape coexistence of the oblate and prolate states in ^{28}Si . One of the unique features in ^{24}Ne is that

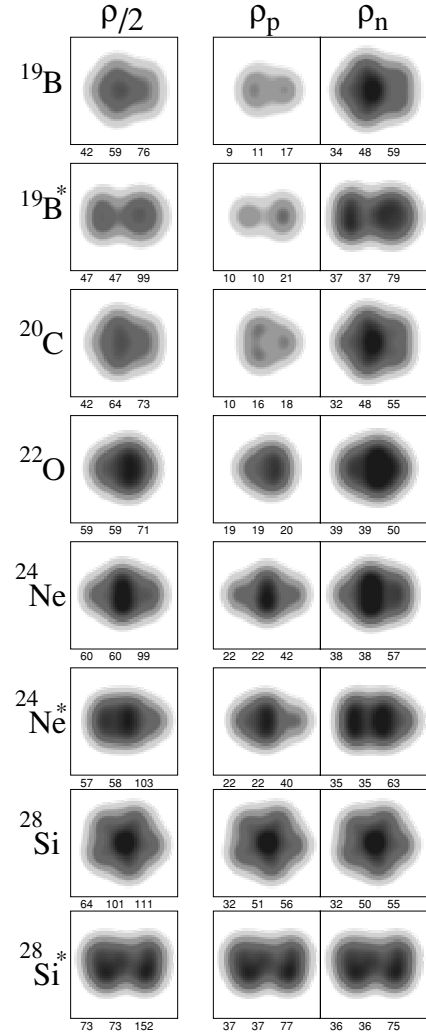


FIG. 6. Density distribution of the intrinsic state $\Phi_{\text{AMD}}(\mathbf{Z})$. The axis of the intrinsic frame are chosen as $\langle xx \rangle \leq \langle yy \rangle \leq \langle zz \rangle$ and $\langle xy \rangle = \langle yz \rangle = \langle zx \rangle = 0$. The intrinsic system is projected onto the zy plane. The density is integrated along the transverse axis x . The densities for matter, protons, and neutrons are displayed in the left, middle, and right panels, respectively. $\langle xx \rangle$, $\langle yy \rangle$, $\langle zz \rangle$ for matter, proton, and neutron densities are written below the figures. The unit of the box frame size is 10×10 fm.

the proton deformations are prolate in both the ground and excited states. It is because of the nature of $Z = 10$ systems. Due to the effect of prolate proton deformation, the oblate neutron structure varies into the small prolate deformation. As a result, the deformation parameters β_p and β_n for the proton and neutron densities are inconsistent with each other as $\beta_p > \beta_n$. This leads to a difference between proton and neutron deformations in the ground state of ^{24}Ne . The details of the different deformations are discussed later in relation to the $E2$ transition strengths.

In the results of ^{28}Si , the oblate and prolate states coexist. As already mentioned, the oblate feature of the ground state is reproduced with the stronger spin-orbit force ($u_{ls} = 2800$ MeV). The shape coexistence of ^{28}Si has been studied by 7α -cluster

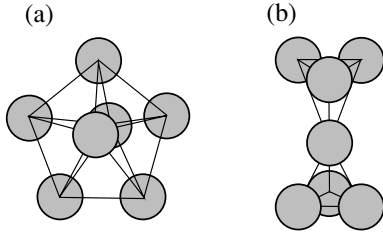


FIG. 7. Schematic figures for the positions (\mathbf{D}_i) of the Gaussian centers in the oblate (a) and prolate (b) states of ^{28}Si . The positions \mathbf{D}_i ($i = 1 \sim 28$) are distributed in seven groups that associate with the 7α -cluster configurations.

models [10–12], where exotic shapes have been suggested in addition to the normal oblate and prolate deformations. For example, a pentagon shape composed of 7α clusters with D_{5h} symmetry [12] is attributed to the $K^\pi = 5^-$ rotational band that has been observed in gamma transition measurements [4]. In the present calculations, all the centers of 28 single-nucleon Gaussians are treated as independent variational parameters without assuming existence of any cluster cores. By analyzing the positions \mathbf{D}_i ($i = 1 \sim 28$) of Gaussian centers, we find that the oblate and prolate states consist of 7α -like clusters in the present results. Schematic figures for spatial configurations of the oblate and prolate states are shown in Fig. 7. Due to the 7α clustering, the pentagon shape appear in the oblate solution as seen in Fig. 6. We give a comment on “ α ” clusters in the present results. Because the imaginary parts of the single-nucleon Gaussian centers are nonzero in the oblate solution, the α -like clusters are *dissociated* α clusters, which differ from the ideal α clusters written by $(0s)^4$ harmonic-oscillator wave functions. The details are discussed in the last part of this section.

B. ^{19}B

The structure of B isotopes has been studied with the AMD method in Ref. [13]. In the previous results, it was predicted that cluster structure develops as a neutron number increases from ^{13}B toward the neutron-drip line ^{19}B due to a large prolate deformation of neutron structure. In the present results, however, the ground state of ^{19}B has the oblate neutron structure, which is inconsistent with the previous results. In the previous calculations of ^{19}B , the oblate solution was not lower than the prolate solution because the adopted spin-orbit force $u_{ls} = 900$ MeV was too weak. As explained, the relative energy of the prolate and oblate solutions is sensitive to the strength of spin-orbit force. Therefore, it is important to use a proper strength of the spin-orbit force to describe the feature of shape coexistence in $N = 14$ systems. By using the stronger spin-orbit force $u_{ls} = 2800$ MeV, which can reproduces the level scheme of the oblate and prolate bands in ^{28}Si , the oblate band becomes lowest in ^{19}B , whereas the prolate band appear as the excited band (Fig. 2). As a result, the neutron structure of the ground state of ^{19}B is predicted to be oblate in the present work. The oblate property of the ground band of ^{19}B is contrast to the features of other neutron-rich B isotopes (^{15}B and ^{17}B), where prolate neutron structure is favored [13].

Because of the oblate neutron structure in ^{19}B , the proton deformation is smaller, and the clustering is weaker in the ground state than the excited prolate state as seen in Fig. 6. The deformation of the neutron structure is reflected in the electric quadrupole moment (Q) through the proton deformation. As shown in Table III, the calculated $Q(3/2^-)$ for the oblate ground state is much smaller than that for the prolate excited state. The experimental measurement of the Q moment of ^{19}B is required to confirm the oblate neutron deformation. Contrary to the Q moments, the calculated magnetic dipole moments μ are not so much different between oblate and prolate states.

C. ^{24}Ne

^{24}Ne is an interesting nucleus, because the proton structure in $Z = 10$ system may favor a prolate shape as known in ^{20}Ne . Considering the coexistence of oblate and prolate shapes in $N = 14$ neutron structure, it is natural to expect that the neutron shape and the proton shape may compete. The present results suggest that the different kinds of neutron structure coexist in ^{24}Ne . One is the smaller prolate deformation in the ground band, and the other is the larger prolate deformation in the excited band. The former is attributed to the oblate structure in the $N = 14$ systems. We consider that the change of the neutron structure from the oblate shape into the small prolate deformation is understood as the oblate neutron structure is somehow soft and is varied by the prolate nature of the proton structure. The present results suggest the smaller neutron deformation β_n than the proton deformation β_p as $\beta_n < \beta_p$ in the ground band of ^{24}Ne . Conversely, β_n is as large as β_p in the excited band.

To extract information about the proton and neutron deformations from the experimental data, it is useful to analyze $E2$ transition strengths and compare them with those of mirror nuclei. Similar analyses on the electric moments were done in Refs. [26,27], where deformations of C isotopes have been discussed. Recently, $B(E2; 2_1^+ \rightarrow 0_1^+)$ in ^{24}Si has been measured by Coulomb excitation [7] as $B(E2) = 4.6 \pm 1.4$ w.u., which is smaller than or of same order of $B(E2; 2_1^+ \rightarrow 0_1^+) = 6.8 \pm 1.6$ w.u. in ^{24}Ne . If we assume the mirror symmetry between ^{24}Ne and ^{24}Si , $B(E2; ^{24}\text{Si})$ in ^{24}Si should be equal to $B_n(E2; ^{24}\text{Ne})$ for neutron transitions in ^{24}Ne . Therefore, these facts suggest that, in ^{24}Ne , the neutron transition strength $B_n(E2; ^{24}\text{Ne})$ is as small as the proton transition strength $B(E2; ^{24}\text{Ne})$. The ratio $B_n(E2; ^{24}\text{Ne})/B(E2; ^{24}\text{Ne}) \leq 1$ is smaller than the naive expectation, $(N/Z)^2 \approx 2$, given by a collective model picture. The reduction of $B_n(E2; ^{24}\text{Ne})$ can be described by the smaller neutron deformation β_n than the proton deformation β_p in the “oblate” ground band. In fact, the calculated ratio $B_n(E2)/B(E2) = B(E2; ^{24}\text{Si})/B(E2; ^{24}\text{Ne})$ in the “oblate” band of ^{24}Ne is approximately 1 (Table II), which agrees well with the experimental data. Conversely, in the excited prolate band with $\beta_n \approx \beta_p$, the calculated $B(E2; ^{24}\text{Si}^*)$ is twice as large as the $B(E2; ^{24}\text{Ne}^*)$, and the ratio $B_n(E2)/B(E2) = B(E2; ^{24}\text{Si}^*)/B(E2; ^{24}\text{Ne}^*)$ is consistent with the collective model expectation $(N/Z)^2 \approx 2$. Comparing the calculations and the experimental data of $B(E2; ^{24}\text{Ne})$ and $B(E2; ^{24}\text{Si})$,

we conclude that the ‘‘oblate’’ band correspond to the ground band of ^{24}Ne . The present result of the ‘‘oblate’’ band still overestimates the $B(E2; ^{24}\text{Si})$ as shown in Table II. It is conjectured that the neutron deformation might be smaller due to the $d_{5/2}$ shell closure effect.

D. Lowering mechanism of oblate states

The shape coexistence in ^{28}Si has been studied by 7α -cluster models for a long time [10,11]. The oblate and prolate solutions coexist as local minima in the α -cluster model space; however, most of the calculations fail to reproduce the order of the oblate and prolate states in ^{28}Si . Even in the three-dimensional calculations of 7α clusters, the prolate solution is lower than the oblate solution [11], which is inconsistent with the fact of the oblate ground state. Exceptions are the 7α calculations with a few parameter sets of Brink-Boeker forces in Ref. [10], though the binding energy is greatly underestimated.

The main reason for the failures in describing the deformation of the ground state of ^{28}Si in the 7α -cluster calculations is because the spin-orbit force is omitted in the α -cluster models. As seen in the Nilsson orbits [6], the spin-orbit force plays an important role to make the shell gap at $N = 14$ in the oblate system. It means that the spin-orbit force is necessary to gain the energies of the oblate states in $N = 14$ systems. Here we explain the lowering mechanism of the oblate state in ^{28}Si within the AMD model space.

As described in Sec. VA, in the results of ^{28}Si it is found that the positions \mathbf{D}_i (the real part of \mathbf{X}_i/\sqrt{v}) of Gaussian centers correspond to the 7α -like cluster configurations (Fig. 7). If the imaginary parts of the Gaussian centers are zero, the expectation value of the spin-orbit force vanishes because it is exactly zero in the systems composed of the ideal $(0s)^4$ - α clusters. However, in the intrinsic state of the oblate band, we find that the nonzero imaginary parts of the Gaussian centers cause the rotational motion. The positions and the momenta of the single-nucleon Gaussian wave packets are given by the real parts $\{D_y\}_i$ and imaginary parts $\{K_x\}_i$ of the Gaussian centers (\mathbf{X}_i/\sqrt{v}) as given in Eq. (5). $\{D_y\}_i$ and $\{K_x\}_i$ in the intrinsic state of the oblate ground band of ^{28}Si are plotted in Fig. 8. The positions and momenta for up-spin and down-spin nucleons are shown by square and circle points, respectively. The correlation between D_y and K_x indicates the rotational motion around the z axis. Namely, the angular momenta of the up-spin nucleons are parallel to the z axis and those of the down-spin nucleons are antiparallel. Therefore, the rotational motions for up-spin nucleons and the down-spin nucleons are reverse to each other and make the spin-orbit force attractive. The energy gain of the spin-orbit force is more than 20 MeV as shown in Table I. In the k th α -like cluster, the momenta $K_x(\uparrow)$ for the up-spin proton and neutron are opposite to those $K_x(\downarrow)$ for the down-spin proton and neutron as $K_x(\uparrow) = -K_x(\downarrow)$ as shown in Fig. 8. Although the positions \mathbf{D}_i are located in the 7α -like cluster configurations, it is important that the α -like clusters are dissociated due to the imaginary parts \mathbf{K}_i , because the Gaussians for the up-spin nucleons are moving

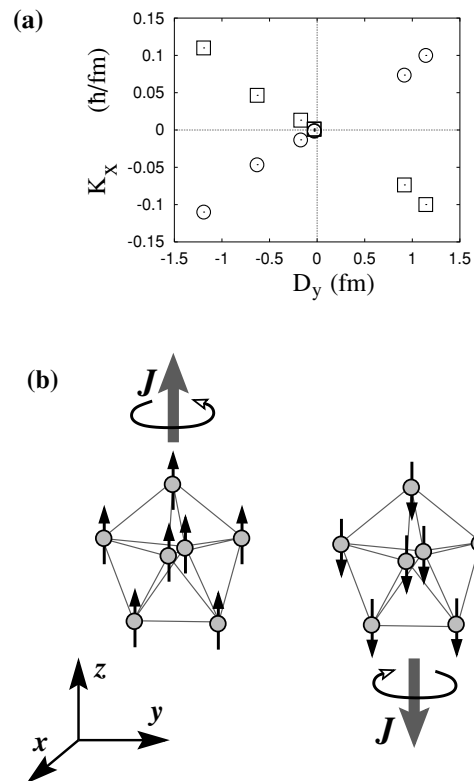


FIG. 8. (a) Positions D_y and momenta K_x of 28 Gaussian centers in the intrinsic wave function of the oblate solution of ^{28}Si . The x , y , and z axes are chosen to be $\langle x^2 \rangle \leq \langle y^2 \rangle \leq \langle z^2 \rangle$. The z axis in the oblate solution almost equals the direction of the intrinsic-spins of single-nucleon wave functions. (b) Schematic figure for the rotational motion given by the positions and momenta of Gaussian centers.

in the reverse to the down-spin nucleons in each of α -like clusters.

Thus, in the AMD framework, the spin-orbit force can increase while maintaining the α -like cluster configurations. The energy gain of the spin-orbit force arises from the flexibility of the AMD wave functions where Gaussian centers are expressed by ‘‘complex’’ variational parameters instead of real parameters.

VI. SUMMARY

We studied the deformations of $N = 14$ isotones, ^{19}B , ^{20}C , ^{22}O , ^{24}Ne , and ^{28}Si , while focusing on the shape coexistence of the oblate and prolate neutron structure. The relative energies between the oblate and prolate states are found to be sensitive to the strength of spin-orbit force. By using a set of interaction parameters $m = 0.62$ and $u_{ls} = 2800$ MeV in the MV1(case 1)+G3RS force, we can describe the properties of the shape coexistence in ^{28}Si , which is known to have the oblate ground band and the prolate excited band. The present results agree reasonably with the experimental data of radii, moments, and $E2$ transition strengths.

In the present calculations, the solutions with the oblate neutron structure are energetically favored and form the ground bands in these $N = 14$ isotones. In the results of ^{19}B , the prolately deformed excited band with cluster structure was predicted to appear above the oblate ground state. In ^{24}Ne , we proposed a possible difference between proton and neutron deformations in the ground band. We discussed Q moments and $E2$ transition strengths in relation to the intrinsic deformations. In the analysis of the results, it was found that the spin-orbit force plays an important role in the lowering mechanism of the oblate neutron structure in $N = 14$ systems. We found that the imaginary parts of the single-nucleon Gaussian centers in the AMD model space are important to gain the spin-orbit force.

ACKNOWLEDGMENTS

The author thanks Professor H. Horiuchi, Professor K. Ikeda, and Dr. M. Kimura for many discussions. She is also thankful to Professor T. Motobayashi for valuable comments. The computational calculations in this work were supported by the Supercomputer Project Nos. 70, 83, and 93 of the High Energy Accelerator Research Organization (KEK). This work was supported by the Japan Society for the Promotion of Science and a Grant-in-Aid for Scientific Research of the Japan Ministry of Education, Science and Culture. The work was partially performed in the ‘‘Research Project for Study of Unstable Nuclei from Nuclear Cluster Aspects’’ sponsored by Institute of Physical and Chemical Research (RIKEN).

-
- [1] S. Das Gupta and M. Harvey, Nucl. Phys. **A94**, 602 (1967).
 [2] D. Pelte *et al.*, Phys. Lett. **B29**, 660 (1969).
 [3] G. C. Ball *et al.*, Nucl. Phys. **A349**, 271 (1980).
 [4] F. Glatz, P. Betz, J. Siefert, F. Heidinger, and H. Röpke, Phys. Rev. Lett. **46**, 1559 (1981); F. Glatz *et al.*, Z. Phys. A **303**, 239 (1981).
 [5] W. Sun, Y. Watanabe, E. Sh. Sukhovitskiĭ, O. Iwamoto, and S. Chiba, J. Nucl. Sci. Technol. **40**, 635 (2003).
 [6] A. Bohr and B. R. Mottelson, *Nuclear Structure*, Vol. 2 (Benjamin, New York, 1975).
 [7] S. Kanno *et al.*, Prog. Theor. Phys. Suppl. **146**, 575 (2002).
 [8] G. Leander and S. E. Larsson, Nucl. Phys. **A239**, 93 (1975).
 [9] A. L. Goodman, G. L. Struble, J. Bar-Touv, and A. Goswami, Phys. Rev. C **2**, 380 (1970).
 [10] W. Bauhoff, H. Schultheis, and R. Schultheis, Phys. Rev. C **26**, 1725 (1982).
 [11] J. Zhang, W. D. M. Rae, and A. C. Merchant, Nucl. Phys. **A575**, 61 (1994).
 [12] W. Bauhoff, Z. Phys. **305**, 187 (1982).
 [13] Y. Kanada-En’yo, H. Horiuchi, and A. Ono, Phys. Rev. C **52**, 628 (1995); Y. Kanada-En’yo and H. Horiuchi, Phys. Rev. C **52**, 647 (1995).
 [14] Y. Kanada-En’yo and H. Horiuchi, Prog. Theor. Phys. Suppl. **142**, 205 (2001).
 [15] Y. Kanada-En’yo, M. Kimura, and H. Horiuchi, C. R. Acad. Sci., Ser. B, **4**, 497 (2003).
 [16] G. Thiamova, N. Itagaki, T. Otsuka, and K. Ikeda, Nucl. Phys. **A719**, 312c (2003).
 [17] D. M. Brink, in *Many-body Description of Nuclear Structure and Reactions*, International School of Physics ‘‘Enrico Fermi,’’ Varenna, 1965, Course 36, edited by C. Bloch (Academic, New York, 1966), p. 247.
 [18] T. Neff and H. Feldmeier, Nucl. Phys. **A738**, 357 (2003).
 [19] R. Roth, T. Neff, H. Hergert, and H. Feldmeier, Nucl. Phys. **A745**, 3 (2004).
 [20] Y. Kanada-En’yo, Phys. Rev. Lett. **81**, 5291 (1998).
 [21] T. Ando, K. Ikeda, and A. Tohsaki-Suzuki, Prog. Theor. Phys. **64**, 1608 (1980).
 [22] N. Yamaguchi, T. Kasahara, S. Nagata, and Y. Akaishi, Prog. Theor. Phys. **62**, 1018 (1979); R. Tamagaki, Prog. Theor. Phys. **39**, 91 (1968).
 [23] A. Ozawa *et al.*, Nucl. Phys. **A691**, 599 (2001), and references therein.
 [24] H. de Vries *et al.*, At. Data and Nucl. Data Tables **36** (1987).
 [25] S. Raman *et al.*, At. Data and Nucl. Data Tables **36** (1987).
 [26] Y. Kanada-En’yo and H. Horiuchi, Phys. Rev. C **55**, 2860 (1997).
 [27] Y. Kanada-En’yo, Phys. Review C (to be published).